Michael Hoff (Autor)

Stewartson layers, inertial waves and wave instabilities in a spherical-gap flow

Laboratory experiments with full optical access

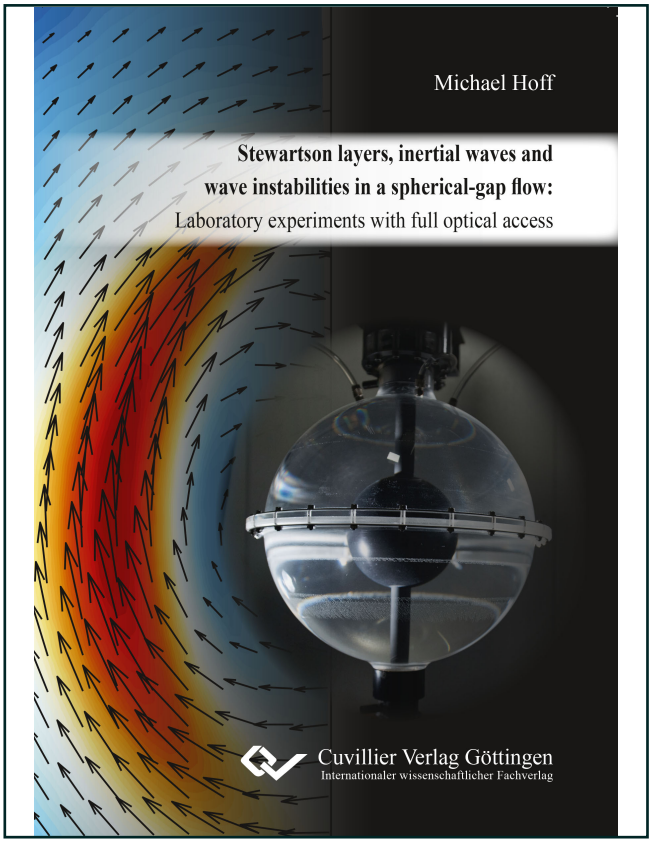

https://cuvillier.de/de/shop/publications/7640

Chapter 1

Introduction

1.1 Why spherical-gap geometry?

Many planetary bodies in our solar system consist of a solid inner and a liquid outer core, surrounded by a 'solid' shell (the outer spherical shell). The region between two such concentric spheres is called *spherical gap*. Such fluid-filled spherical gaps are omnipresent in nature. The most obvious example is given by our Earth (Fig. 1.1). But also other planets, like Mercury, Jupiter and Saturn, as well as the Earth's moon and the Galilean moons of Jupiter consist of spherical-gap geometry (see e.g. Spohn, 2007). In principle, the Earth consists of different layers (Fig. 1.1), so-called spherical shells, which are separated with respect to their density distribution but also to their particular dynamical and chemical processes (rotation, convection, tectonics, etc.). The solid inner core, the liquid outer core, the mantle and the crust (continental as well as oceanic) build the basis of the Earth's structure. The atmosphere, particularly the troposphere, and the oceans represent an outer fluid layer, dominated by large and small-scale dynamical motions as well. Because of these different layers, several fields of applications of spherical gaps can be noticed (see Tab. 1.1). Assuming that the tropopause is a boundary where,

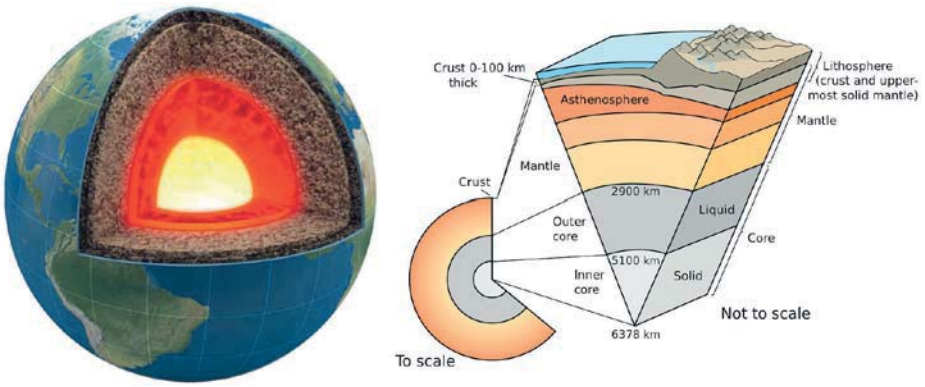

FIGURE 1.1: Image of the Earth and its different layers. Picture taken from Kious *et al.* (1996).

inner sphere	*outer shell*	*gap-filling fluid*	*relevant for*
continental crust	tropopause	moist air mixture	Meteorology
ocean crust	ocean surface	saline water	Oceanography
solid iron core	**lower mantle**	**molten metal**	Geophysics/ Astrophysics

TABLE 1.1: Examples of spherical gaps on the Earth.

for example, waves get reflected, the troposphere forms a very thin spherical gap, for which the continental crust forms the inner sphere. This behaves similarly for the ocean and the oceanic crust. From theoretical models of the equatorial ocean and atmospheric dynamics, there remain large uncertainties since most of the models make use of the traditional approximation that neglects the vertical component of the Coriolis force. Laboratory and numerical experiments in spherical-gap geometry are not affected by this kind of approximations and might hence form a testbed for the subtle equatorial dynamics of geophysical flows (see e.g. Harlander and Maas, 2006, 2007a, Rabitti and Maas, 2013, 2014, Rabitti, 2016). However, in terms of the radius ratio, the present work is more related to thick spherical gaps like the Earth's core. It has a radius ratio of about $r_\mathrm{i}/r_\mathrm{o} \approx 0.35$ (Spohn, 2007), being r_i and r_o the inner and outer sphere radius, which is close to $r_\mathrm{i}/r_\mathrm{o} = 1/3$ used for the present work.

The Earth's core is one of the most inaccessible places in the universe. The Kola borehole is the deepest borehole in the history of exploration of the Earth's interior. However, with a depth of $\sim 12\,\mathrm{km}$ it just 'scratches' the surface, considering that the inner core begins at around 2900 km depth. In contrast, gravimetrical analysis and measurements of seismic activities are indirect methods to determine, for example, the density of the inner core or its spin rate. But also volcanic activity and the structure of meteorites can be used to obtain information about the Earth's interior. Despite all these efforts, most of the structure and dynamical behaviour of the Earth's core remains uncertain and unknown. Therefore, it is indispensable to use alternatives like spherical-gap models (theoretically, numerically and experimentally) to investigate the dynamics and underlying mechanisms of the Earth's liquid outer core, and eventually extrapolate certain aspects to planetary scales with the help of scaling laws.

One particular property of spherical gaps, like planetary cores, is that they do not rotate constantly since there is additional forcing. There are three main periodic forcing mechanisms: (i) precession, which is a periodic variation of the rotation vector, (ii) tidal forcing, which is a periodic variation in shape, and (iii) longitudinal libration, which is a superposed oscillation on the rotation speed. A rather steady forcing, which is roughly related to libration, is steady differential rotation for which the inner core and outer shell rotate constantly at different speeds. Many planetary bodies and satellites, like Mercury, the Earth's moon or the Galilean moons of Jupiter librate due to interactions with their gravitational partners (see e.g. Comstock and Bills, 2003). The Earth's core, on the other hand, undergoes a slight differential rotation ($\mathcal{O}(10^{-6})$) where the inner core and outer mantle rotate at different speeds. This happens due to a strong

gravitational coupling between the mantle and the inner core where small fluctuations of the mantle momentum have a strong impact on the inner core's rotation (Aldridge and Lumb, 1987, Rieutord, 1995). One source for such fluctuations is proven to be strong earthquakes (Song and Richards, 1996, Buffett, 1997). Apart from planetary-shaped bodies, also accretion disks are driven by differential rotation (Li *et al.*, 2000, 2001) and can approximately be modelled by spherical gaps. Two review articles about fluid motions in spheres, spherical gaps and spheroids have recently been published by Le Bars *et al.* (2015) and Le Bars (2016).

All these rotational background systems have a significant influence on the fluid in the interior of planets and stars. It is worth to know the interaction between the core rotation and the interior of the fluid to understand, for example, tidal heating, fluid mixing, and the generation of magnetic fields. About the importance and the recent necessity of investigations of pure rotational effects, Le Bars *et al.* (2015) stated the following: For more than half a century most research on fluid dynamics in planetary liquid core models focused on convective processes. The main purpose of this past research was to demonstrate that convective flows in a rotating spherical gap can generate a dynamo. Most notably the magnetic field of the Earth is caused by such motions. However, it is difficult to validate these models with observational data since sufficiently high temperature gradients cannot be reached neither by laboratory experiments nor by numerical models, or, obtained standard scaling laws fail to extrapolate to real astrophysical systems. Moreover, Le Bars *et al.* (2015) noted that it is often assumed that fluid motions in astrophysical bodies are controlled and driven by convective effects only. However, in situ data from space missions of the last couple of years imply that there is a huge reservoir of energy stored in the rotational motion of planets and stars which can sustain intense large-scale flows. Therefore, studies on pure rotational effects in planetary core shaped models gain increasing attention (the reader is referred to Le Bars *et al.*, 2015, Le Bars, 2016, for more detailed information).

Moreover, they stated that the mechanical forcings, which are small compared to the overall rotation, do not directly provide the energy to drive particular flows. They act more as conveyors that extract a part of the potential rotational energy and transfer it to intense large-scale fluid motions. Such motions can be inertial waves or wave modes (e.g. in the Earth's liquid outer core, Aldridge and Lumb, 1987, Rieutord, 1995) and Stewartson shear layers (Stewartson, 1957, 1966, Hide and Titman, 1967, Früh and Read, 1999, Hollerbach, 2003, Koch *et al.*, 2013, Sauret and Le Dizès, 2013). Even more, this energy transfer gives rise to various types of instabilities (e.g. elliptical instability, shear instability or centrifugal instability) which are the topics of the present work. Of particular interest are wave interactions and Stewartson layer instabilities (Hide and Titman, 1967, Hollerbach, 2003, Hollerbach *et al.*, 2004, Schaeffer and Cardin, 2005a,b, Wicht, 2014).

An opportunity to explore aspects of the dynamics and mechanisms in planets and stars is to do laboratory experiments. Usually, planets, atmospheres and oceans are complex systems with a

high degree of physical processes and variables. Therefore, it is necessary to confine investigations to certain aspects of the flow. Thus, the main motivation of performing spherical gap flow experiments is to simplify the entire system of a planetary core and focus on observations and excitation mechanisms of certain phenomena. Moreover, experiments are not affected by assumptions, theoretical restrictions and approximations and are hence helpful to validate numerical and analytical models, or to find new aspects of flows. Laboratory experiments are also necessary from a fluid dynamical point of view. The Navier-Stokes equation might, to some extent, accurately cover the flow dynamics, however, analytical solutions do not exist for all fluid dynamical problems. This concerns especially inertial waves in spheres and spherical gaps, which are investigated in this work.

For these reasons, we conduct various experiments in an isothermally rotating fully transparent spherical-gap flow experiment with a radius ratio of $\eta = r_\mathrm{i}/r_\mathrm{o} = 1/3$ in order to improve previous findings, to find new flow phenomena, and to validate numerical simulations in collaboration with the Max Planck Institute of Solar System Research in Göttingen (A. Barik, Group of J. Wicht) and S. A. Triana from the Royal Observatory of Belgium in Brussels. Our apparatus can imitate differential rotation and inner sphere libration. The latter has been used to study inertial waves, wave interactions and instabilities under controlled forcing conditions (Koch *et al.*, 2013). Of special interest is the wave reflection behaviour at inclined walls which can be studied using simple ray models (Greenspan, 1968, Tilgner, 1999, Harlander and Maas, 2006, Borcia and Harlander, 2013, Koch *et al.*, 2013). From such models, as well as from experiments and numerical simulations, it is known that for spherical gaps energy can be focused on closed orbits and wave attractors (Tilgner, 1999, Maas, 2001, Rieutord *et al.*, 2001, Harlander and Maas, 2006, Rabitti and Maas, 2013, 2014).

As could be demonstrated more recently, differential rotation in a spherical gap gives rise to intense large-scale motions, called inertial modes. These modes resembled eigenmodes known analytically and experimentally from full spheres and spherical gaps (Aldridge, 1967, 1972, Zhang *et al.*, 2001). Our studies revealed a new secondary instability of inertial modes characterised by a clear and abrupt transition to weak small-scale turbulence.

A rather steady feature which exists for both forcing systems is the Stewartson layer. In spherical gaps, the Stewartson layer forms a vertical cylinder parallel to the axis of rotation touching the inner sphere's equator (Stewartson, 1957, 1966, Hollerbach, 2003, Koch *et al.*, 2013, Sauret and Le Dizès, 2013). For a critical shear, i.e. when the libration amplitude or the differential rotation exceeds a certain threshold, this layer becomes unstable. Such shear flow instabilities are of general geophysical interest, for example in meteorology (barotropic Rossby waves), oceanography (gulf stream), and astrophysics (Jovian jet) since they contribute to angular momentum transport and mixing processes.

1.2 About this thesis

The main body of the present thesis is based on two published articles (Hoff *et al.*, 2016a,c) and a third manuscript in writing process (Hoff and Harlander, 2017). We suggest two ways to read the thesis: first sequentially, following the storyline over all nine chapters, or second, reading the results parts separately (Chapters 6, 7 and 8). Each of these three chapters is based on a published article or unpublished manuscript, i.e. it has an introduction, methods, results and discussion. It is therefore written self-contained for convenience of both, the reader and the author. If more detailed information about theory or measurement techniques is required while reading, the reader is referred to the respective previous chapter.

Following the content of the three main articles, the thesis consists of the experimental investigation of three different flow phenomena which mainly occur in an isothermally rotating spherical gap flow; Stewartson layers and their instabilities (Hoff *et al.*, 2016a, Hoff and Harlander, 2017), inertial wave shear layers excited by an external periodic mechanical forcing (Hoff *et al.*, 2016a), and propagating inertial modes excited by steady differential rotation forcing (Hoff *et al.*, 2016c). All these flow features can be caused by pure rotational effects, without applying an external heating or cooling. To drive them in our spherical-gap apparatus, we use two main forcing mechanisms. The first is libration of the inner sphere, which is a superposed sinusoidal oscillation on the mean rotation rate of the inner sphere. This is called periodic mechanical forcing, such as precessional or tidal forcing. The second is differential rotation for which the inner and outer sphere rotation rates are different. In contrast to libration, differential rotation is a rather steady forcing. However, it is able to drive significant shear flows which might become unstable, leading to inertial oscillations in the fluid. The flowchart in Fig. 1.2 illustrates the addressed flow features and how they are related to the rotational forcings.

The storyline of the thesis is as follows:

This thesis begins with the theoretical background in Chapter 2. The content of this chapter is mainly taken from textbooks and builds the basis of understanding the investigated flow phenomena from a theoretical point of view. We examine the underlying basic equations and derive relevant properties of inertial waves, like the group and phase velocity, as well as their reflection behaviour. We further discuss limiting cases of inertial waves with high and low frequencies. Especially low-frequency inertial waves play a significant role in a spherical-gap flow.

The second part of Chapter 2 focuses on contained inertial waves in spheres and spherical gaps. If no external forcing is applied, contained inertial waves, so-called inertial modes, are the eigenmodes of the system. We summarise the inviscid theory of inertial modes in a full sphere from Greenspan (1968), since it has recently been shown that inertial modes also exist in a spherical gap (Kelley *et al.*, 2007, 2010, Triana, 2011). If external periodic forcing is applied, inertial waves in a spherical gap consist of distinct shear layers. From all past studies, a huge variety

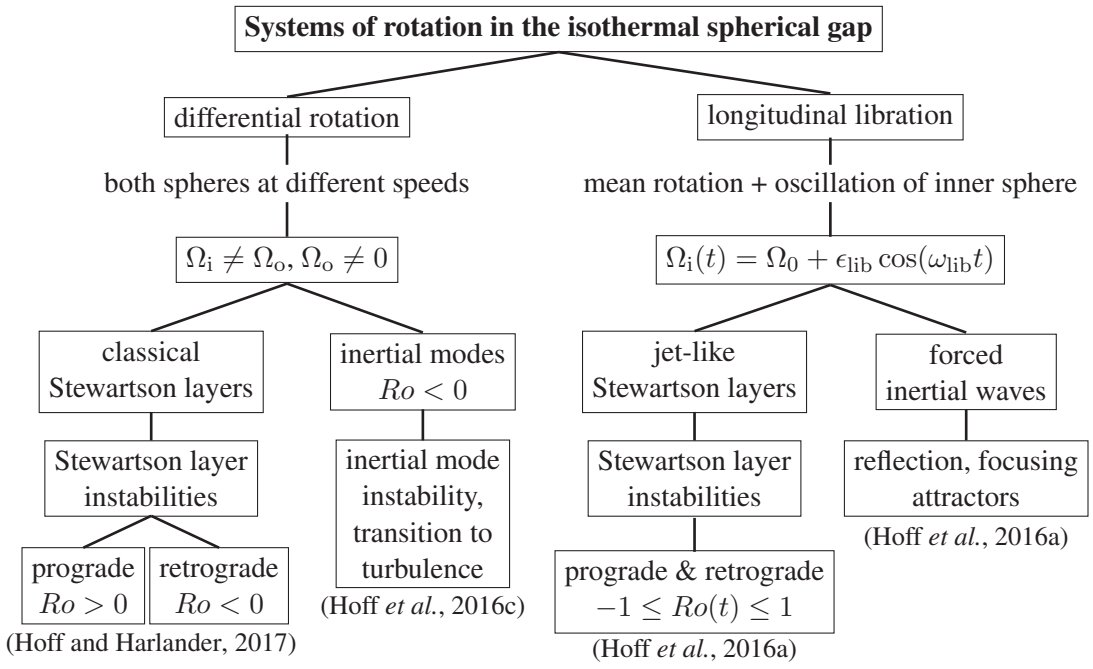

FIGURE 1.2: Flow chart illustrating the two different rotational systems investigated in this thesis.

of scaling laws arose about the width of the shear layers, the velocity magnitude and several transitional effects (instabilities). We extract the most important scalings which are helpful to classify our experimentally observed phenomena.

The experimental setup is described in Chapter 3. Since detailed technical information about the device is given in Dahley (2016), we will only briefly recall the most important features. Instead, we focus on the efficiency of the implemented libration mechanism, since this is helpful in understanding the dependency of inertial wave shear layers on the libration parameters. Also part of this chapter is the description of a thorough calibration of all the rotational systems, i.e. inner and outer sphere rotation rate, solid-body rotation, differential rotation, as well as inner sphere libration. This helps not only to determine the exact rotation rates, but also to deeply understand how the applied background rotations operate.

The next chapter concerns the visualisation of the flow in the spherical gap. Since the working fluid is transparent, and we are operating in a closed system, it is profitable to inject tracer particles into the fluid, which can then be illuminated using a laser-light-sheet technique. Chapter 4 describes two measurement techniques. In the meridional plane, we measure the flow qualitatively to get a rough picture of the flow phenomena. This method has been used in several studies (e.g. Koch *et al.*, 2013, Klein *et al.*, 2014, Seelig, 2014). The new contribution to the present spherical-gap experiment is the design of a small co-rotational particle-image-velocimetry (PIV) system to extract a two-dimensional and two-component (2D2C) velocity field in the horizontal plane. From this, we can derive plenty of dynamical features, like divergence, vorticity or

Reynolds-stresses. Therefore, we will describe in detail the setup of this PIV system and the equipment used, as well as its processing via the Matlab toolbox MatPIV (Sveen, 2004, Sveen and Cowen, 2004), followed by a detailed error estimation.

It is very difficult to extract key-dynamical features of the visualised flow without applying statistical post-processing tools. In Chapter 5, we describe the theoretical background of all relevant statistical methods, as well as the application of these methods to our data. All described methods need a sufficiently long time-series to give qualitatively reliable results. In detail, the fast Fourier transform (FFT) can be used to detect significant frequencies time series. The harmonic analysis is a least-square technique for which known frequencies in a time series can be used to derive the corresponding amplitude and phase information, i.e. a harmonic oscillation. It has successfully been applied to similar data in Klein *et al.* (2014) and Seelig (2014). However, the harmonic analysis is not the most appropriate choice if one is interested in normal modes of the system. The empirical orthogonal function (EOF) analysis is a tool to derive 'statistical modes' of the system, which are often similar to normal modes (Hoff *et al.*, 2015). Further, we describe how to estimate principle oscillation patterns (POPs), and singular vectors (SVs) since they are useful to determine pattern growth. All these methods have been improved for the application to experimental geophysical data (Hoff *et al.*, 2015) and they give a decisive access into the dynamics of a system, which cannot be detected by other methods.

A new method applied to data where many wave interactions are assumed, is the so-called bispectral analysis. With the help of this statistical tool, nonlinear wave couplings can qualitatively be detected. Bispectral analysis has a long list of applications since the 1970s, however, it receives increasing attention in geophysically related laboratory experiments, especially where internal waves in rotating or stratified fluids are investigated. We outline its theory in Chapter 5.

In Chapter 6, 7 and 8, we present the experimental results. Chapter 6 focuses on Stewartson layers (SL) and their instabilities. Two different structures of SL's could be noticed (see 1st and 3rd branch of the flowchart in Fig. 1.2): The classical SL excited by differential rotation and a jet-like SL excited by inner sphere libration. There is a huge amount of numerical and experimental studies concerning SL's in different geometries, for example in cylinders with rotating disks (Hide and Titman, 1967, Früh and Read, 1999), spheres with polar 'caps' (Schaeffer and Cardin, 2005a,b). However, quantitative experimental studies with full optical access are scarce. Therefore, we extensively discuss the structure of both SL's in our spherical gap. Due to increasing shear rate, the SL can become unstable. We found that a large set of low-frequency waves, so-called Rossby waves, get excited. Their dependency on the dimensionless parameters, their structure, their mutual interaction, as well as their interaction with the mean flow could be derived. This offers a new contribution on understanding these features and their existence. Herewith, we could answer some open questions, however, other questions cannot be answered

by performing laboratory experiments only. This concerns especially physical mechanisms, which can be extracted easier from numerical simulations.

Chapter 7 deals with plane inertial waves directly forced by inner sphere libration (4th branch of the flow chart in Fig. 1.2). This was also the topic of Koch *et al.* (2013) and Dahley (2016), but using a larger radius ratio, $r_\mathrm{i}/r_\mathrm{o} = 1/2$. We made a similar study to highlight the key facts about inertial wave shear layers and their reflection in a spherical gap. For comparison, we make use of a geometrical two-dimensional ray-tracing model in the meridional plane. The focus in this chapter, however, lies on quantitative results. From an energetic point of view, we discuss inertial wave shear layers in the gap and possible influences from the background flow. Once the flow is supercritical, i.e. SL instabilities occur, plane inertial waves interact nonlinearly with the low-frequency Rossby waves, leading to a subset of secondary waves induced by triadic resonances.

Inertial modes driven by differential rotation (2nd branch of the flow chart in Fig. 1.2) are discussed in Chapter 8. Since the last decade it is known that some of those inertial modes get excited in a spherical gap when the inner sphere rotates slower than the outer shell (Kelley *et al.*, 2007, 2010, Triana, 2011, Rieutord *et al.*, 2012). Surprisingly, despite the strong background flow, their structure agreed well with analytical full-sphere modes (Zhang *et al.*, 2001). However, a comprehensive quantitative survey of the modes was technically impossible since those previous spherical-gap flow experiments have been performed in opaque shells. Therefore, not much is known about the underlying dynamics, especially how and under which conditions they get excited and how they interact with the background flow. For these reasons, we give a comprehensive view on the interior structure of the detected inertial modes and compare them qualitatively with reports from the literature. Another important question concerns the Ekman number dependency. The Ekman number, $E = \nu/(\Omega_\mathrm{o}\, d^2)$, where ν is the viscosity, Ω_o the outer shell rotation rate and d the gap width, describes the ratio between viscous and Coriolis forces. In this context, we should pre-empt that our experiment runs at much larger Ekman numbers than the other spherical gap experiments ($\mathcal{O}(10^{-5})$ in our study compared to $\mathcal{O}(10^{-7})$ in Kelley *et al.* (2007, 2010), Triana (2011) or Rieutord *et al.* (2012)). Due to this, we enter a completely different regime which predominantly leads to different results. A lucky coincidence of performing at these smaller Ekman numbers is that we observed a remarkable and sharp transition from a more regular regime (with many discrete wave events) to a weakly turbulent regime (with a more continuous wave spectrum and less discrete peaks). Before and beyond this transition, the flow exhibits remarkable properties. Since such a transition could not be observed in previous differentially rotating spherical gap flows, the second and largest part of Chapter 8 largely focuses on related flows features from an energetic point of view. We further suggest possible mechanisms which can cause such a transition to turbulence. However, a definite statement can only be made with the help of numerical simulations, which are planned for future work. To confirm, at least, some of our observations, preliminary results of numerical simulations from

A. Barik Barik *et al.* (2017), a Ph.D. student at the Max Planck Institute of Solar System Research (MPS) in Göttingen and S. A. Triana from the Royal Observatory of Belgium will be presented.

Finally, a conclusion will be made in Chapter 9. We summarise the results and revisit the most important, newly acquired findings of the present work and set them in the latest scientific context. An outlook with suggestions for future investigations completes this thesis.

Chapter 2

Fundamentals

2.1 Equations of motion

Consider a fluid parcel which moves with a velocity $\vec{v} = \vec{v}(\vec{x}, t)$, where $\vec{x} = (x, y, z)$ is the space vector in a Cartesian coordinate system and t is the time. Such a moving parcel can be described by the three Newton's laws of motion. For every force acting on a fluid parcel additionally holds the superposition principle,

$$\frac{\mathrm{d}\vec{v}}{\mathrm{d}t} = \frac{1}{m}\sum_{\mathrm{i}} \vec{F}_{\mathrm{i}} = \sum_{\mathrm{i}} \vec{a}_{\mathrm{i}}. \tag{2.1}$$

In (2.1), $\vec{F}_{\mathrm{i}}$ and $\vec{a}_{\mathrm{i}}$ are the individual forces and accelerations acting on a fluid parcel, and $\mathrm{d}/\mathrm{d}t$ is the total (individual) temporal derivative, given by

$$\frac{\mathrm{d}}{\mathrm{d}t} = \frac{\partial}{\partial t}\frac{\mathrm{d}t}{\mathrm{d}t} + \frac{\partial}{\partial x}\underbrace{\frac{\mathrm{d}x}{\mathrm{d}t}}_{u} + \frac{\partial}{\partial y}\underbrace{\frac{\mathrm{d}y}{\mathrm{d}t}}_{v} + \frac{\partial}{\partial z}\underbrace{\frac{\mathrm{d}z}{\mathrm{d}t}}_{w}, \tag{2.2}$$

where ∂ denotes the partial derivative. Reshaping (2.2) leads to

$$\underbrace{\frac{\mathrm{d}}{\mathrm{d}t}}_{\text{total}} = \underbrace{\frac{\partial}{\partial t}}_{\text{local}} + \underbrace{\vec{v}\cdot\nabla}_{\text{advection}}. \tag{2.3}$$

Possible forces (or accelerations) which can act on a fluid parcel are, among others, pressure gradient forces, gravitational forces and viscosity forces. In a rotating frame of reference, there are also acting apparent forces, like Coriolis force or centrifugal forces. In the following, we describe the forces which are important for this thesis and build our particular equations of motions. For detailed information, the reader is referred to Greenspan (1968), Pedlosky (1987, 2003) or Holton (2004).

2.1.1 Pressure gradient acceleration

The pressure gradient acceleration is denoted by $\vec{a}_{\mathrm{pre}}$. Whenever a pressure gradient ∇p is present, an acceleration will act on a particular fluid parcel in the direction of $-\nabla p$, i.e. from high to low pressure. Consider a fluid volume $\delta^3 V = \delta x \delta y \delta z$, the pressure along the x-axis acting from left is given by $F_{\mathrm{pre}} = p\, A = p\, \delta y \delta z$ and the pressure acting from right is given by $F_{\mathrm{pre}} = (p + \frac{\partial p}{\partial x}\delta x)\, \delta y \delta z$. The net force acting on the fluid volume along the x-direction is given by

$$\delta F = -\frac{\partial p}{\partial x}\delta V. \tag{2.4}$$

Dividing (2.4) by δm and using of $\rho = \delta m / \delta V$, where ρ is the density, we obtain

$$a_{\mathrm{pre}} = \frac{\delta F_{\mathrm{pre}}}{\delta m} = -\frac{\partial p}{\partial x}\,\frac{\delta V}{\delta m} = -\frac{1}{\rho}\,\frac{\partial p}{\partial x}. \tag{2.5}$$

Considering all three dimensions, we get

$$\vec{a}_{\mathrm{pre}} = -\frac{1}{\rho}\,\nabla p. \tag{2.6}$$

The gradient always points towards the direction of the strongest increase. The minus sign in (2.6) implies that the pressure gradient force is directed to lower pressure. Thus, a fluid parcel is accelerated along the direction of the strongest pressure decrease.

2.1.2 Gravitational acceleration

The general form of Newton's gravitational acceleration is given by $\vec{a}_{\mathrm{gra}}$ with

$$\vec{a}_{\mathrm{gra}} = -\frac{G\,M}{r^2}\frac{\vec{r}}{r} \equiv \vec{g}_{\mathrm{N}}, \tag{2.7}$$

with M as the Earth's mass and G the gravitational constant and $r \approx R = 6371\,\mathrm{km}$ the radius of the Earth. Usually, $\vec{g_{\mathrm{N}}}$ depends on the height z in the atmosphere, however, z mostly small compared to the Earth's radius. Further, $\vec{g}_{\mathrm{N}}$ can be written in terms of the gravitational potential $\phi_{\mathrm{gra}} = G\,M/r$, via its gradient

$$\nabla\phi_{\mathrm{gra}} = G\,M\,\nabla\frac{1}{r} = -G\,M\,\frac{1}{r^2}\cdot\frac{\vec{r}}{r} = \vec{g}_{\mathrm{N}}. \tag{2.8}$$

2.1.3 Friction acceleration

The friction acceleration is denoted by $\vec{a}_{\mathrm{fri}}$. Friction always acts opposite to the motion of a fluid parcel and is a measure of the resistance of the motion. The most common source of friction

acceleration in fluid dynamics is due to viscosity of the fluid. The following statements are captured from Holton (2004).

In a Newtonian fluid, the viscous force in x-direction per unit area, or shearing stress, in an incompressible fluid can be defined as (Holton, 2004)

$$\tau_{\mathrm{zx}} = \lim_{\delta z \to 0} \mu \frac{\delta u}{\delta z} = \mu \frac{\partial u}{\partial z}. \tag{2.9}$$

In a more general case, we consider a small but finite fluid volume element with lengths $\delta x \delta y \delta z$. The shearing stress in x-direction acts through the centre of the element and is designated τ_{zx}. The stress acting across the upper boundary on the fluid below can be written approximately as

$$\tau_{\mathrm{zx}} + \frac{\partial \tau_{\mathrm{zx}}}{\partial z} \frac{\delta z}{2} \tag{2.10}$$

and the stress acting across the lower boundary on the fluid above is

$$- \left[\tau_{\mathrm{zx}} - \frac{\partial \tau_{\mathrm{zx}}}{\partial z} \frac{\delta z}{2} \right]. \tag{2.11}$$

The net viscous force on the volume element acting in x-direction is then given by

$$\left[\tau_{\mathrm{zx}} + \frac{\partial \tau_{\mathrm{zx}}}{\partial z} \frac{\delta z}{2} \right] \delta x \delta y - \left[\tau_{\mathrm{zx}} - \frac{\partial \tau_{\mathrm{zx}}}{\partial z} \frac{\delta z}{2} \right] \delta x \delta y. \tag{2.12}$$

Dividing by $\rho \, \delta x \delta y \delta z$ gives the viscous force per unit mass due to vertical shear of the component of motion in x-direction

$$\frac{1}{\rho} \frac{\partial \tau_{\mathrm{zx}}}{\partial z} = \frac{1}{\rho} \frac{\partial}{\partial z} \left(\mu \frac{\partial u}{\partial z} \right). \tag{2.13}$$

Considering the stress acting in all other directions and assuming μ to be constant (which is approximately the case in this thesis), we get

$$\vec{a}_{\mathrm{fri}} = \nu \nabla^2 \vec{v}, \tag{2.14}$$

where $\nu = \mu / \rho$ is the kinematic viscosity with $[\nu] = \mathrm{m}^2 \, \mathrm{s}^{-1}$.

2.1.4 Apparent accelerations

In an absolute (inertial) reference frame, the above described Newton's laws of motion are valid. However, when rotation comes into play, a relative (rotating) coordinate system is considered and additional forces are acting. Thus, to obtain the absolute acceleration of the fluid velocity in a rotating coordinate system, the basis vectors $(\hat{i}, \hat{j}, \hat{k})$ are moving and their derivative is non-zero. On the Earth, for example, the time-variation of the basis vectors is a function of the Earth's rotation $\vec{\Omega}_{\mathrm{E}}$ with

$$\frac{\mathrm{d}\vec{r}}{\mathrm{d}t} = \vec{v}_\mathrm{r} = \vec{\Omega}_\mathrm{E} \times \vec{r}. \tag{2.15}$$

After some rearrangements, we obtain for the velocity $\vec{v}_\mathrm{a}$ in the absolute coordinate system (e.g. Pedlosky, 1987)

$$\vec{v}_\mathrm{a} = \vec{v} + \vec{\Omega}_\mathrm{E} \times \vec{r}. \tag{2.16}$$

After some algebraic rearrangements (see, e.g. Pedlosky (1987) for detailed information) we get for the absolute acceleration of the velocity

$$\frac{\mathrm{d}\vec{v}_\mathrm{a}}{\mathrm{d}t} = \frac{\mathrm{d}\vec{v}}{\mathrm{d}t} + \underbrace{2\vec{\Omega} \times \vec{v}}_{\mathrm{I}} + \underbrace{\vec{\Omega} \times (\vec{\Omega} \times \vec{r})}_{\mathrm{II}} + \underbrace{\frac{\mathrm{d}\vec{\Omega}}{\mathrm{d}t} \times \vec{r}}_{\mathrm{III}}, \tag{2.17}$$

where $\vec{\Omega}$ is the rotation vector of the system considered. From (2.17), it is obvious that three additional forces are acting in a rotating system: the Coriolis force (I), the centrifugal (or centripetal) force (II) and variations in the rotation rate itself (III).

I. The Coriolis acceleration is denoted by $\vec{a}_\mathrm{cor} = -2\vec{\Omega}\times\vec{v}$. This apparent force is responsible for the deflection of moving fluid particles (or objects) due to rotation. In case of the Earth, objects will be deflected to the right in the northern hemisphere and to the left in the southern hemisphere. Further simplifications can be made when aligning the x-axis of the local coordinate system with the longitudinal direction. Then the x-component of the rotation vector is zero and we get

$$\vec{a}_\mathrm{cor} = -2\vec{\Omega} \times \vec{v} = -\begin{pmatrix} f^\star\, w - f\, v \\ f\, u \\ -f^\star\, u \end{pmatrix}, \tag{2.18}$$

where $f = 2\,\Omega \sin\varphi$ and $f^\star = 2\,\Omega \cos\varphi$ and φ being the latitude. In the mid-latitudes, the vertical component of the velocity, w, is small compared to the horizontal components. Then, (2.18) can be further simplified. This assumption can be made, for example, when horizontal wind models are considered (Pedlosky, 1987, Holton, 2004).

II. The centrifugal acceleration is denoted by $\vec{a}_\mathrm{cen} = -\vec{\Omega} \times (\vec{\Omega} \times \vec{r})$. With a geometric interpretation (see Pedlosky, 1987, Fig.1.6.1), $\vec{a}_\mathrm{cen}$ can be rewritten and considered in terms of a potential function, ϕ_cen, with

$$\vec{a}_\mathrm{cen} = -\vec{\Omega} \times (\vec{\Omega} \times \vec{r}) = |\vec{\Omega}|^2 \vec{r}_\perp = \nabla\phi_\mathrm{cen}, \quad \text{with} \quad \phi_\mathrm{cen} = \frac{|\vec{r}_\perp|^2 |\vec{\Omega}|^2}{2}. \tag{2.19}$$

Hence, we can summarise the potential force due to centrifugal forces and the potential due to gravity forces, mentioned in (2.8), to a total potential force,

$$\nabla\Phi = \nabla\phi_{\mathrm{gra}} + \nabla\phi_{\mathrm{cen}}. \tag{2.20}$$

III. The variation of the rotation rate itself is negligible for most oceanographic or atmospheric phenomena except for those whose time scales are unusually long (Pedlosky, 1987). For our experiments, Ω is a constant.

2.1.5 The Navier-Stokes equation

The first basic equations which are needed for the mathematical description of our fluid flow are the equations of motion, i.e. the Navier-Stokes equations. They represent the conservation of momentum in a fluid. The classical form of the Navier-Stokes equation for an incompressible fluid in an inertial frame of reference (without rotation) reads

$$\frac{\mathrm{d}\vec{v}}{\mathrm{d}t} = \frac{\partial\vec{v}}{\partial t} + (\vec{v}\cdot\nabla)\vec{v} = -\frac{1}{\rho}\nabla p + \vec{g}_{\mathrm{N}} + \nu\nabla^2\vec{v}. \tag{2.21}$$

A particular feature in (2.21) is the nonlinear term, the advection of the velocity vector. This term has the form

$$(\vec{v}\cdot\nabla)\vec{v} = \begin{pmatrix} u\frac{\partial u}{\partial x} & + & v\frac{\partial u}{\partial y} & + & w\frac{\partial u}{\partial z} \\ u\frac{\partial v}{\partial x} & + & v\frac{\partial v}{\partial y} & + & w\frac{\partial v}{\partial z} \\ u\frac{\partial w}{\partial x} & + & v\frac{\partial w}{\partial y} & + & w\frac{\partial w}{\partial z} \end{pmatrix}, \tag{2.22}$$

or can be reshaped via a vector rule (Weber-transformation)

$$(\vec{v}\cdot\nabla)\vec{v} = \frac{1}{2}\nabla(\vec{v}\cdot\vec{v}) - \vec{v}\times(\nabla\times\vec{v}). \tag{2.23}$$

If rotation, and hence apparent forces, come into play, the equations of motion change to

$$\frac{\mathrm{d}\vec{v}}{\mathrm{d}t} = \frac{\partial\vec{v}}{\partial t} + (\vec{v}\cdot\nabla)\vec{v} = -\frac{1}{\rho}\nabla p + \nabla\Phi - 2\vec{\Omega}\times\vec{v} + \nu\nabla^2\vec{v}. \tag{2.24}$$

Often, for simplicity, in fluid dynamics the pressure and the potential forces are summarised in the so-called modified pressure gradient $\nabla p' = \nabla p + \nabla\phi_{\mathrm{gra}} + \nabla\phi_{\mathrm{cen}}$.

2.2 The continuity equation

The second basic equation which is needed for the mathematical description of our fluid flow is the continuity equation. The continuity equation is based on the conservation of mass, $\mathrm{d}m/\mathrm{d}t = 0$. It says that the net mass flux density through a volume element, $\delta^3V = \delta x\,\delta y\,\delta z$, i.e. the